Processing and Application of Ceramics 11 [2] (2017) 93–99
https://doi.org/10.2298/PAC1702093R

Compacting and densification of TiO_2 nanoparticles

Roman Alvarez Roca*, Edson Roberto Leite, Elson Longo

LIEC-DQ, Federal University of São Carlos, São Carlos-SP, 13656-905, Brazil

Received 12 December 2016; Received in revised form 24 February 2017; Received in revised form 7 April 2017; Accepted 17 April 2017

Abstract

This work investigated the compacting and densification behaviour of TiO_2 nanoparticles prepared by the simple non-aqueous sol-gel process. The synthesized nanopowder has anatase TiO_2 structure with the average crystallite size of 10 nm and agglomerated particles. The compressibility curve shows two well-defined linear parts that intersect at ~380 MPa which is a measure of agglomerate compressive strength. The densification process was investigated by the dilatometric analysis using non-isothermal experiments. The apparent activation energy for the densification was calculated (88–102 kJ/mol). Grain rearrangement by grain boundary sliding was proposed as the dominant shrinkage mechanism.

Keywords: *titania, agglomerates, nanopowders, sintering*

I. Introduction

The consolidation and sintering of nanomaterials have attracted the attention on different aspects of materials processing [1–4]. The consolidation of ultrafine powder is difficult, not only because of its high surface area relative to its weight and severe interparticles friction, but also due to the high degree of agglomeration. This powder ability to agglomerate is due to the Van der Waals attraction. A low and inhomogeneous distribution of the density is expected within a green body during the compaction of a highly agglomerated powder. This degree of inhomogeneity has a significant impact on its subsequent densification behaviour. For improving the ceramic sinterability, the pressure- and field-assisted sintering methods have been applied [2,4–6]. However, many of these techniques are not economically attractive, depending on the use of the final product. Thus, conventional pressureless sintering is still an attractive method to produce ceramics, mainly due to its simplicity and lower cost compared to the other methods [7–13]. Preventing these undesirable agglomeration effects is one of the major challenges in the ceramic processing via conventional sintering. An optimal compaction pressure, adequate control of the heating curve as well as different firing schedules could be used to achieve this purpose. In addition, the factors and mechanisms controlling densification should be perfectly identified in order to improve the sinterability and material properties [2,5,6,14–16].

In this work, the compacting and densification behaviour of TiO_2 nanoparticles prepared by a simple non-aqueous route was studied. The effect of agglomeration status was investigated by the density-pressure curve, dilatometric analysis, using non-isothermal experiments and microstructural examination.

II. Experimental procedure

The reagents, purchased from Aldrich company, consisting of 3.3 ml titanium chloride ($TiCl_4$) and 30 ml of polytetramethylene ether glycol (terathane, M_w = 1000) were mixed, with molar ratio of 1:2, in a dry box under controlled atmosphere. The reaction was conducted in the silicone oil bath at 120 °C for 72 hours and the detailed procedure was reported earlier [17]. The final powder was washed, dried and characterized by X-ray diffraction (XRD) using a Rigaku D/MAX-2500 diffractometer. The microstructure was analysed by a transmission electron microscope (TEM) model TECNAI F20 (FEI Company, Eindhoven, Netherlands) operating at 200 kV. Before compacting, the powder was calcined to eliminate the organics. The calcination was conducted separately at two temperatures, 400 °C and 600 °C, (samples denoted as T400 and T600, respectively) for 2 hours. For compressibility studies, the powders were

* Corresponding author: tel: +55 16 33518214,
fax: +55 16 33518208, e-mail: *cortes116@yahoo.es*

uniaxially compacted into pellets (10 mm diameter) at different compacting pressures between 150 MPa and 2 GPa using a stainless-steel die. The green samples were heated up to 1400 °C in air with constant heating rates (CHR) of 10, 20 and 25 °C/min for the densification kinetics studies by dilatometric analysis. The shrinkage of the compacts was analysed with high temperature horizontal dilatometer NETZSCH - DIL 402 PC (Netzsch-Gerätebau GmbH) coupled with the temperature control TASC 414/3 under air flow. For the microstructural analysis the green bodies were non-isothermally sintered by conventional sintering (CS) at temperatures between 950 and 1400 °C in air, with a heating rate of 10 °C/min. The two-step sintering (TSS) technique was used, too. For the first step of TSS, pellets were heated up to a higher temperature, T_1, with a heating rate of 10 °C/min. After being held at T_1 for t_1 = 1 min, they were cooled down to a lower temperatures, T_2, with a cooling rate of 40 °C/min and soaked at T_2 for a prolonged time, t_2. Different TSS schedules (Table 1) were performed by the combination of different values of T_1, T_2 and t_2. The sintered samples (i.e. well-polished surface with thermal etching) were observed using an Inspect F50 field-emission scanning electron microscope (FEG-SEM, model FEI Company, Hillsboro) with an operating range of 5–15 kV. The densities of both samples, green and sintered, were calculated and measured from the geometric (measuring weight and dimensions of the compacts) and Archimedes methods, respectively. For relative density determination, the theoretical density values 3.89 and 4.24 g/cm^3 were used for anatase and rutile, respectively. The grain size was calculated from the micrographs using a linear intercept technique.

III. Results and discussion

3.1. Powder and green pellet characterisation

The XRD pattern of the as-synthesized products is presented in Fig. 1. The data confirm the tetragonal-structured anatase TiO_2 (which is in good agreement with the JCPDS, card No. 21-1272) and no characteristic peaks of other phases. The average crystallite size, measured by high-resolution TEM (HRTEM) and calculated by XRD pattern using Scherrer equation, was approximately 10 nm. TEM image of the as-synthesized powder, Fig. 2, confirms that the powder consists of very fine particles with irregular geometry, but clusters of particles can also be clearly observed, indicating the presence of agglomeration.

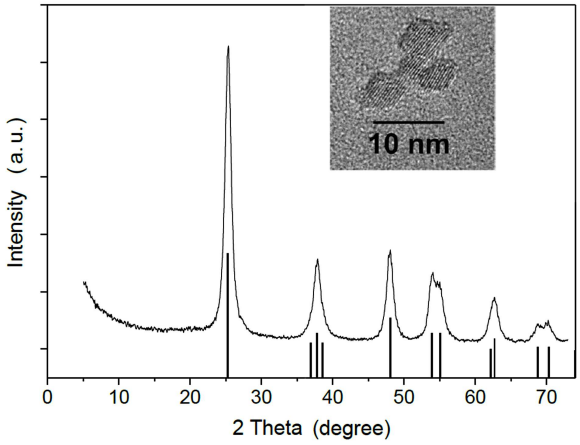

Figure 1. XRD pattern of the as-synthesized TiO_2 powder (HRTEM image of nanoparticles with coherent match between them at the interfaces is inserted)

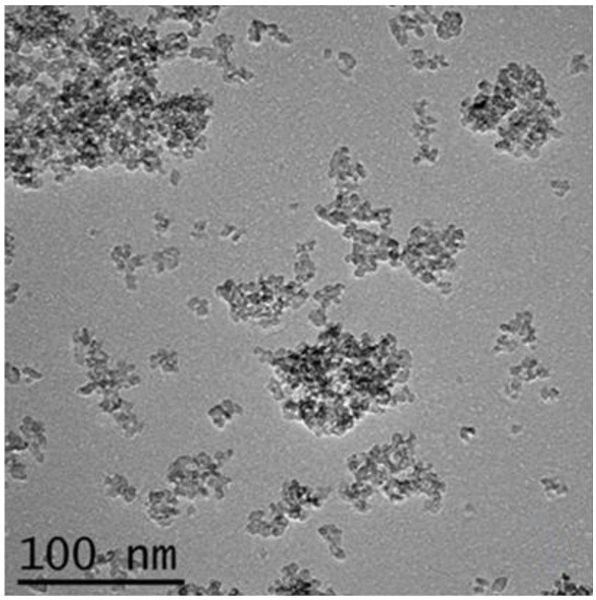

Figure 2. TEM micrographs of the as-synthesized TiO_2 powder

Table 1. Cycle details used for CS and TSS and relative densities of sintered samples

Regime	T_1 [°C]	t_1 [min]	T_2 [°C]	t_2 [h]	RD [%TD]
CS	1000	1	-	-	82.2
	1150	1	-	-	87.1
	1250	1	-	-	89.5
	1400	1	-	-	91.1
TSS	1000	1	950	20	86.0
	1150	1	1050	4	90.4
	1250	1	1150	4	90.9
	1250	1	1150	10	92.8
	1250	1	1200	4	90.1
	1400	1	1300	4	93.2

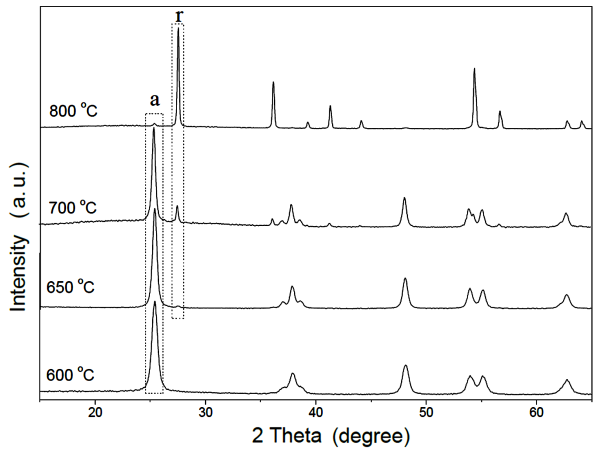

Figure 3. XRD patterns of the TiO_2 powders calcined at various temperatures for 2 h (a - the most intense anatase peak, r - the most intense rutile peak)

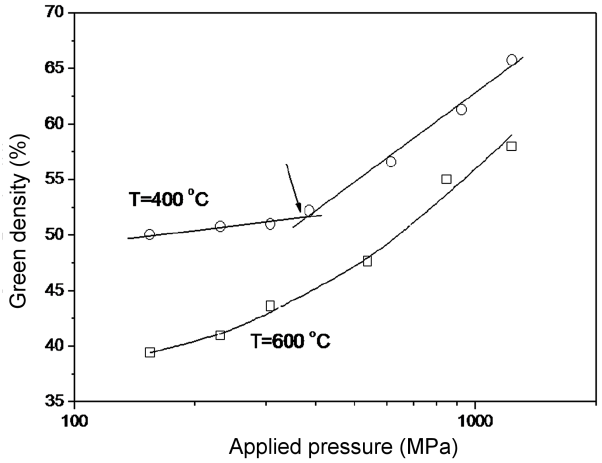

Figure 4. Green density plotted vs. logarithm of compaction pressure at calcination temperatures of 400 °C (○) and 600 °C (□)(arrow indicates the agglomerate strength)

Figure 3 shows the XRD difractograms of the TiO_2 powders after calcination at various temperatures for 2 hours. It can be seen that the XRD pattern of the TiO_2 powder calcined at 600 °C contains all the reflection peaks of anatase phase. The reflections were broad due to the crystallite sizes being in the nanometer range. All the reflections in the XRD pattern of the TiO_2 powder after calcination at 650 °C still belong to the anatase phase, except the most intense 110 peak of TiO_2 rutile, which appeared with very weak intensity. Anatase-rutile mixed phase is seen after calcination at 700 °C (Fig. 3), in which the anatase phase is still maintained and other peaks of rutile appear. With successive raise in the calcination temperature, the anatase and rutile phases were coexisting, the rutile reflections become stronger and the intensity of anatase reflections decrease. After calcination at 800 °C, the rutile peaks are strong and the anatase reflections practically disappear, which indicates that the anatase phase is fully converted to rutile. This behaviour indicates that the anatase-to-rutile phase transition occurs between 600 and 800 °C. Approximately the same range is observed for other nanostructured TiO_2 materials [18–21].

The plots of the relative density of the green compact as a function of the logarithm of compaction pressure for the samples T400 and T600 are displayed in Fig. 4. For the T400 sample, the curve shows two linear parts with a point of intersection (or breaking point) at P_b pressure. According to the previous investigations on agglomerated nanopowder compaction, P_b is a measure of the agglomerate strength [8,9,22,23]. At compaction pressures above P_b, the agglomerates are fragmented, while below P_b they are only rearranged. In this work, the value of P_b is around 380 MPa, which is much higher than the value of 37 MPa reported for TiO_2 by Mazaheri *et al.* [8]. Nevertheless, it is similar in range, or even lower, than the values reported for other nanooxides prepared by different chemical methods (Table 2) [9,22,23].

For the T600 sample, with lower green density, the curve is not completely linear, and it is not possible to identify the breaking point. This behaviour might be explained with a higher calcination temperature promoting intra-agglomerate sintering, which makes agglomerates strong enough that they cannot be broken. The formation of agglomerates is related to the coalescence of the nanoparticles during precipitation and drying, via collision and adhesion of colloidal particles. Recently, we showed that these colloidal particles form agglomerates (i.e. anatase TiO_2 mesocrystals) via oriented attachment mechanism [17]. For our samples, the formation of hard agglomerates can be related to the surface-modifier effects and by enhanced interfacial adhesion of the particles by the oriented attachment. By increasing the calcination temperature, surface diffusion can be activated and promote formation of necks between particles. This leads to the sintering within agglomerate, resulting in an increase in aggregate strength. The obtained results confirmed that the agglomerate strength strongly depends on the synthesis method, structure (size and packing of the primary particles, porosity, etc.), thermal history and intrinsic mechanical properties.

3.2. Shrinkage and densification kinetic

Before sintering studies, dilatometric and densification kinetics analyses were performed. A dilatometric plots (linear shrinkage, $\psi = \Delta L/L_0$, and the linear shrinkage rate, $d\psi/dt$, as a function of the temperature) of the T400 sample heated up to 1000 °C are shown in Fig. 5. The presence of two peaks, P1 and P2, was observed in the densification rate curve for the samples prepared at pressure bellow P_b (Fig. 5, curve a). These peaks can be related to sintering of intra-agglomerate particles (P1) and sintering of inter-agglomerates (P2). However, for the sample compacted at pressure above P_b (Fig. 5, curve b) only one maximum (P1) in the densification rate curve was observed, which is related only to the sintering of intra-agglomerate particles, as suggested by the compaction behaviour. For this sample the

Table 2. P_b values reported for several nano-oxides

Material	Synthesis method	D^a [nm]	Observation	P_b [MPa]	Ref.
8Y-YSZ	co-precipitation	22	calcinated at 400 °C	80	22
8YSZ	glycine nitrate	24.5	as-synthesized and milled	370	9
CeO_2-8YSZ	co-precipitation	NR	as-synthesized	250	23
CeO_2-8YSZ	co-precipitation	NR	calcinated 350 °C	573	23
TiO_2 (P25, Degussa)	spray pyrolysis	11–27		37	8
TiO_2	solvothermal non-aqueous.	10		380	this work

[a] D is the average particle size
NR – not reported

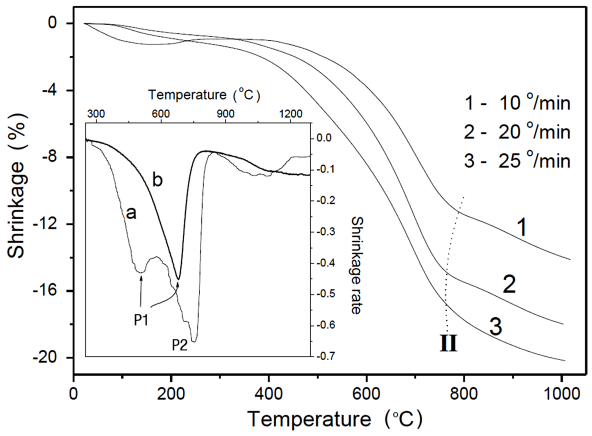

Figure 5. Linear shrinkage ($\psi = \Delta L/L_0$) of nanopowder compacts for different CHRs (insert - the linear shrinkage rate, dψ/dt, at CHR = 10 °C/min, for sample prepared at compaction pressure bellow P_b, curve a, and above P_b, curve b)

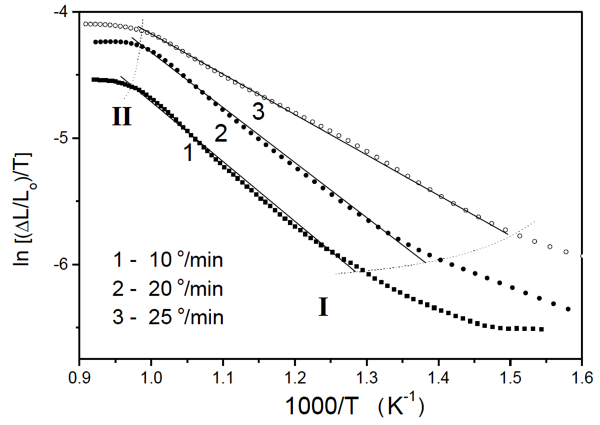

Figure 6. The Arrhenius plots of the ln$\{(\Delta L/L_0)/T\}$ vs. 1/T at different CRHs

agglomerates were broken due to the high compaction pressure (above P_b) and the P2 maximum is suppressed. In the curve b (Fig. 5), the position of P1 peak correlates to the temperature range of the anatase-rutile transformation, and the process can be considered as a phase-transformation assisted sintering process [18,24–26].

Densification kinetics was analysed on the basis of initial sintering theory according to Young and Cutler [27]. The parameters of the densification, such as the activation energy of sintering (Q) and constants related to the sintering mechanism (n), were estimated using equations for densification during a CHR, as reported by Bannister [28] and Han *et al.* [29] and based on the theory given by Young and Cutler [27]. Figure 6 shows Arrhenius plots of experimental data for ln$\{(\Delta L/L_0)/T\}$ vs. $1/T$ at different CHRs. The plots are not completely linear over the whole temperature range, which is expected for compacts having inhomogeneous packing, probably due to the agglomeration. According to this observation, the densification process can be divided into three sections. The first section, up to the dashed line I (see Fig. 6), could be considered as a pre-sintering stage and the shrinkage is fundamentally associated with a gas removed from pores and surface. The second section, between dashed lines I and II, can be related with the initial step of the sintering. After the dashed line II is the third section which is the start of the last sintering step. The values of the Q for the initial step of sintering (the second section between dashed lines I and II) are between 88–102 kJ/mol. The activation energy of sintering was found to be in reasonable agreement with the values reported in the literature: 96.2 kJ/mol [30], 105 kJ/mol [31] and 115 kJ/mol [32]. It can be concluded that the present method can be used to determine activation energy. In accordance with the obtained results several relevant features can be emphasised:

- the nanoparticles sintering occurs at temperatures (for 200 to 400 °C) lower than the sintering of micrometer or submicrometer powders, also well-known for other materials [3,33–36];
- onset shrinkage temperature, T_{os}, is dependent on CHR (dashed line I in Fig. 6), and T_{os} decreases with the increase of the CHR;
- the temperature of the shrinkage rate maxima is practically independent of the CHR;
- shrinkage rate value at the maximum is high (1.33–2.59×10^{-4} s^{-1}) and such high values cannot be explained only by diffusion processes [37,38]. For the diffusion mechanism only, shrinkage rate is supposed to be between 10^{-8}–10^{-5} s^{-1} [39];
- densification is ended at approximately the same temperature, independent of the heating rate, (dashed line II).

For these reasons, we considered that the shrinkage during densification of nanoparticles in the initial sintering step, until 850–900 °C, occurs most probably due to the grain rearrangement by grain boundary sliding.

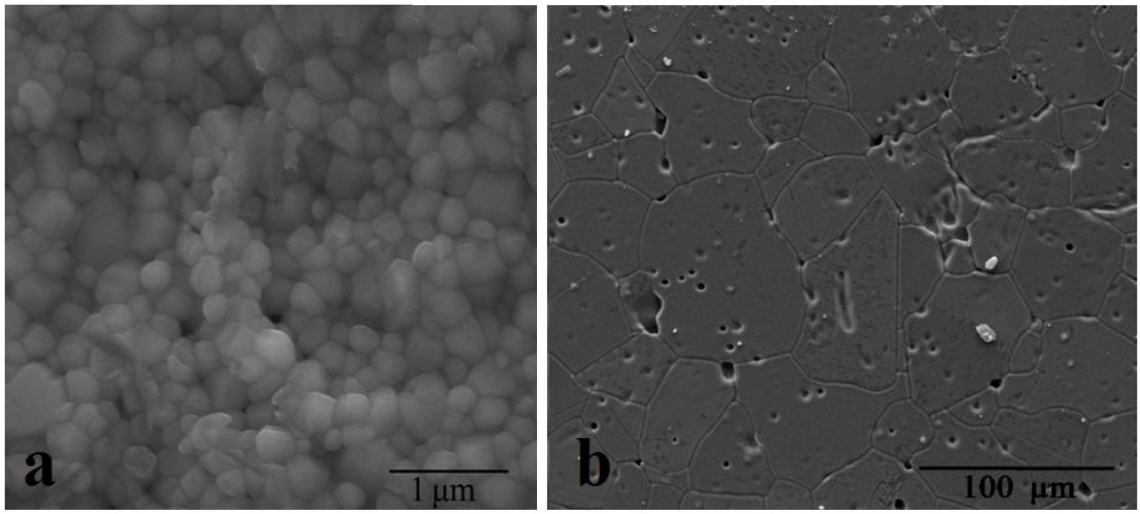

Figure 7. SEM micrograph of the samples sintered by CS at: a) 1000 °C and b) 1400 °C

The slidability requires a certain flexibility of the grain boundary layer, which could be given by a highly disorder status during anatase-rutile transformation. The low value calculated for the activation energy of sintering, lower than for any known pure diffusional mechanism, could be compatible with grain boundary slip assisted by surface diffusion. In addition, the effects of the phase transition on the shrinkage should be considered, too.

3.3. Microstructural analysis

The results of the conventional sintering (CS), one-stage process, for the densities of sintered TiO_2 ceramics at 1000, 1150, 1250 and 1400 °C are summarized in Table 1. Relative densities (RD) were found to be lower than 92 %TD (theoretical density). Usually, 90–92 %TD is assigned as corresponding to the boundary between open and closed porosity [40–42]. This value was not achieved, so it was assumed that a large amount of open pores still remains especially in the samples sintered at lower temperatures.

The microstructures of the polished surfaces of the sintered samples were observed with SEM. The micrographs for the samples sintered at 1000 and 1400 °C are displayed in Fig. 7. It can be seen that the samples have high porosity and non-uniform microstructure. Grains with nanometric scale can be observed for the sample sintered at 1000 °C, (Fig. 7a). The grain diameters are in the range from 100 to 500 nm, but the ceramics has poor densification. When the sintering temperature increases up to 1400 °C, the grain sizes increase abruptly above 30 μm (Fig. 7b). The relative density increases too, and non-uniformity size distribution of the grains and pores was more accentuated.

In order to promote the densification in the nanometric range a two-step sintering (TSS) [7,9,10,26,43] process was applied. The different TSS cycles used and the correspondent RD values obtained are given in Table 1. A slight density increase occurred in relation to CS, but it should be noted that a nearly-fully dense microstructure (RD > 95 %TD) was not reached. Usually, a prerequisite in TSS for successful densification during the second step of this sintering technique is that the pores become sub-critical and unstable against shrinkage [7,44–48]. This stage is reached at 75 %TD and 82 %TD for yittria [7] and alumina [44] nanopowder, respectively. However, these values cannot be accepted as generally valid and our results show that less than 92 %TD is not sufficient for our TiO_2 compacts. A critical microstructure of pores for successful densification depends not only on the porosity value, but also on other pore parameters such as shape, size distribution, mobility, etc.

The low efficiency of the TSS method for removing the final residual porosity can be explained as a consequence of the pore size distributions as well as the particle and/or pore size ratio. At the moment, we neither have an exact explanation for this behaviour, nor for the influence of the stress field promoted by grain boundary sliding. Further experiments are necessary to clarify whether it is caused by the high agglomerate degree, which is more probable, or by the grain boundary slip mechanism, which dominate the initial sintering step according to dilatometric analysis, or by some other effects.

IV. Conclusions

The compacting, densification and sintering of TiO_2 nanoceramic were studied. The experimental results showed that:

- The TiO_2 was synthesized in a nanometric range and the anatase-to-rutile phase transition occurs between 600–800 °C, similar to other nano-TiO_2.
- The compaction curve for the sample calcined at 400 °C shows two well-defined linear parts that intersect at ~380 MPa which is a measure of agglomerate strength.
- Densification kinetics was analysed on the basis of initial sintering theory at different CHR. The values of the Q for the sintering were estimated between 88–102 kJ/mol. We believe that shrinkage is caused by

grain rearrangement due to the grain boundary sliding induced by the anatase-rutile transformation. This densification mechanism is not commonly reported for TiO_2.

- The TEM and densities measurements as a function of sintering temperature displayed that the samples are not fully dense, RD < 92 %TD, which revealed a low efficiency of the low cost processing and sintering methods used in this work. The compaction pressure above P_b and used sintering (CS and TSS) methods are not enough for removing the final residual porosity typical of powder with high agglomeration status.

Acknowledgements: The authors gratefully acknowledge CAPES, CNPq and FAPESP, all Brazilian agencies for providing financial support.

References

1. P.L. Chen, I.W. Chen, "Sintering of fine oxide powders: II, Sintering mechanisms", *J. Am. Ceram. Soc.*, **80** (1997) 637–645.
2. J.R. Groza, "Nanocrystalline powder consolidation methods", Chapter 4 in *Nanostructured Materials: Processing Properties and Potential Applications*, ed. C.C. Koch, 2nd Ed., William Andrew Publishing, New York, 2007.
3. R. Chaim, M. Levin, A. Shlayer, C. Estournes, "Sintering and densification of nanocrystalline ceramic oxide powders: a review", *Adv. Appl. Ceram.*, **107** (2008) 159–169.
4. K. Lu, "Sintering of nanoceramics", *Int. Mater. Rev.*, **53** (2008) 21–38.
5. R.H.R. Castro, K. Benthem, *Sintering - Mechanism of Convention Nanodensification and Field Assisted Processes*, Springer, New York, 2013.
6. Z.H. Zhang, Z.F. Liu, J.F. Lu, X.B. Shen, F.C. Wang, Y.D. Wang, "The sintering mechanism in spark plasma sintering - Proof of the occurrence of spark discharge", *Scripta Mater.*, **81** (2014) 56–59.
7. I.-W. Chen, X.H. Wang, "Sintering dense nanocrystalline ceramics without final-stage grain growth", *Nature*, **404** (2000) 168–171.
8. M. Mazaheri, A.M. Zahedi, M. Haghighatzadeh, S.K. Sadrnezhaad, "Sintering of titania nanoceramic: Densification and grain growth", *Ceram. Int.*, **35** (2009) 685–691.
9. M. Mazaheri, M. Valefi, Z.R. Hesabi, S.K. Sadrnezhaad, "Two-step sintering of nanocrystalline 8 Y_2O_3 stabilized ZrO_2 synthesized by glycine nitrate process", *Ceram. Int.*, **35** (2009) 13–20.
10. D. Li, S.O. Chen, W.Q. Shao, D.C. Wang, Y.H. Li, Y.Z. Long, Z.W. Liu, S.P. Ringer, "Preparation of dense nanostructured titania ceramic using two step sintering", *Mater. Tech.*, **25** (2010) 42–44.
11. C. Liu, L. Miao, J. Zhou, R. Huang, C.A.J. Fisher, S. Tanemura, "Chemical tuning of TiO_2 nanoparticles and sintered compacts for enhanced thermoelectric properties", *J. Phys. Chem. C*, **117** (2013) 11487–11497.
12. Y. Zhang, J. Nie, J. Luo, "Effects of phase and doping on flash sintering of TiO_2", *J. Ceram. Soc. Jap.*, **124** (2016) 296–230.
13. M. Zhou, Z. Huang, J. Qi, N. Wei, D. Wud, Q. Zhang, S. Wang, Z. Feng, T. Lu, "Densification and grain growth of $Gd_2Zr_2O_7$ nanoceramics during pressureless sintering", *J. Eur. Ceram. Soc.*, **37** (2017) 1059–1065.
14. H. Djohari, J.J. Derby, "Transport mechanisms and densification during sintering: II. Grain boundaries", *Chem. Eng. Sci.*, **64** (2009) 3810–3816.
15. J. Koruza, B. Malic, "Initial stage sintering mechanism of $NaNbO_3$ and implications regarding the densification of alkaline niobates", *J. Eur. Ceram. Soc.*, **34** (2014) 1971–1979.
16. P. Guyot, G. Antou, N. Pradeilles, A. Weibel, M. Vandenhende, G. Chevallier, A. Peigney, C. Estournès, A. Maître, "Hot pressing and spark plasma sintering of alumina: Discussion about an analytical modelling used for sintering mechanism determination", *Scripta Mater.*, **84-85** (2014) 35–38.
17. R. Alvarez Roca, E.R. Leite, "Size and shape tailoring of titania nanoparticles synthesized by solvothermal route in different solvents", *J. Am. Ceram. Soc.*, **96** (2013) 96–102.
18. K.P. Kumar, K. Keizer, A.J. Burggraaf, T. Okubo, H. Nagamoto, S. Morooka, "Densification of nanostructured titania assisted by a phase transformation", *Nature*, **358** (1992) 48–51.
19. I.N. Kholmanov, E. Barborini, S. Vinati, P. Piseri, A. Podesta, C. Ducati, C. Lenardi, P. Milani, "The influence of the precursor clusters on the structural and morphological evolution of nanostructured TiO_2 under thermal annealing", *Nanotechnol.*, **14** (2003) 1168–1173.
20. J. Zhang, M. Li, Z. Feng, J. Chen, C. Li, "UV Raman spectroscopic study on TiO_2. I. Phase transformation at the surface and in the bulk", *J. Phys. Chem. B*, **110** (2006) 927–935.
21. S.W. Yeh, Y.L. Chen, C.S. Hsi, H.H. Ko, M.C. Wang, "Thermal behavior and phase transformation of TiO_2 nanocrystallites prepared by a coprecipitation route", *Metall. Mater. Trans. A*, **45** (2014) 261–268.
22. A. Ghosh, K. Ashok, S. Boddapati, T. Rao, T.R. Ramamohan, "Low-temperature sintering and mechanical property evaluation of nanocrystalline 8 mol% yttria fully stabilized zirconia", *J. Am. Ceram. Soc.*, **90** (2007) 2015–2023.
23. A.A. Bukaemskiy, D. Barrier, G. Modolo, "Compressibility and sinterability of CeO_2-8 YSZ powders synthesized by a wet chemical method", *J. Eur. Ceram. Soc.*, **29** (2009) 1947–1954.
24. C. Legros, C. Carry, P. Bowen, H. Hofmann, "Sintering of a transition alumina: effects of phase transformation, powder characteristics and thermal cycle", *J. Eur. Ceram. Soc.*, **19** (1999) 1967–1978.
25. M. Mazaheri, Z.R. Hesabi, S.K. Sadrnezhaad, "Two-step sintering of titania nanoceramics assisted by anatase-to-rutile phase transformation", *Scripta Mater.*, **59** (2008) 139–142.
26. R. Wang, Y. Wang, Z. Fu, H. Wang, W. Wang, J. Zhang, J. Zhu, "Spark plasma sintering of transparent YAG ceramics assisted by the YAH-YAG phase transformation", *J. Eur. Ceram. Soc.*, **36** (2016) 2153–2156.
27. W.S. Young, I.B. Cutler, "Initial sintering with constant rates of heating", *J. Am. Ceram. Soc.*, **53** (1970) 659–663.
28. J.L. Woolfrey, M.J. Bannister, "Nonisothermal techniques for studying initial-stage sintering", *J. Am. Ceram. Soc.*, **55** (1972) 390–394.
29. J. Han, A.M.R. Senos, P.Q. Mantas, "Nonisothermal sintering of Mn doped ZnO", *J. Eur. Ceram. Soc.*, **19** (1999) 1003–1006.

30. Y. Lei, W. Xiong, "Advance in research on nanosintering of ceramic materials", *Mater. Rev.*, **5** (2003) 28–30.
31. S. Chen, Y. Jing, W. Shao, Y. Zhang, W. Luan, D. Li, "The master sintering curve for pressureless sintering of TiO_2", *Sci. Sintering*, **39** (2007) 103–110
32. D. Li, S. Chen, Y. Wan, W. Shao, X. Ge, Y. Zhang, H. Cao, "Apparent sintering activation energy for densification of nanosized TiO_2 ceramic powders", *Mater. Tech.*, **24** (2009) 105–107.
33. M.J. Mayo, "Synthesis and applications of nanocrystalline ceramics", *Mater. Design*, **14** (1993) 323–329.
34. G. Skandan, "Processing of nanostructured zirconia ceramics", *Nanostruct. Mater.*, **5** (1995) 111–126.
35. Z.Z. Fang, H. Wang, "Densification and grain growth during sintering of nanosized particles", *J. Int. Mater. Rev.*, **53** (2008) 326–352.
36. D. Hotza, D.E. García, R.H.R. Castro, "Obtaining highly dense YSZ nanoceramics by pressureless, unassisted sintering", *J. Int. Mater. Rev.*, **60** (2015) 353–375.
37. G.S. Morgan, C.J. McHargue, "Analogies between densification kinetics in sintering and dislocation motion", *Phys. Sintering*, **2** (1970) 55–70.
38. R. Koferstein, L. Jager, M. Zenkner, T. Muller, H.P. Abicht, "Shrinkage mechanism and phase evolution of fine-grain $BaTiO_3$ powder compacts containing 10 mol% $BaGeO_3$ prepared via a precursor route", *Mater. Chem. Phys.*, **112** (2008) 531–535.
39. W. Schatt, *Sintervorgange-Grundlagen*, (*Sintering Processes-Fundamentals* in German), VDI-Verlang, Dusseldorf, 1992.
40. T.M. Shaw, D. Dimos, P.E. Batson, A.G. Schrott, D.R. Clarke, P.R. Duncombe, "Carbon retention in $YBa_2Cu_3O_{7-s}$ and its effect on the superconducting transition", *J. Mater. Res.*, **5** (1990) 1176–1184.
41. J.R. Groza, R.J. Dowding, "Nanoparticulate materials densification", *Nanostruct. Mater.*, **7** (1996) 749–768.
42. C.M. Lapa, F.M.L.R. Figueiredo, F.M.B. Marques, D.P.F. de Souza, "Electrical properties of sub-micrometric ceria-based electrolytes", *Solid State Ionics*, **225** (2012) 424–427.
43. X.H. Wang, X.Y. Deng, H.L. Bai, H. Zhou, W.G. Qu, L.T. Li, I.W. Chen, "Two-step sintering of ceramics with constant grain-size, II: $BaTiO_3$ and Ni-Cu-Zn ferrite", *J. Am. Ceram. Soc.*, **89** (2006) 438–443.
44. J. Li, Y. Ye, "Densification and grain growth of Al_2O_3 nanoceramics during pressureless sintering", *J. Am. Ceram. Soc.*, **89** (2006) 139–143.
45. M. Mikoczyová, D. Galusek, "Influence of forming method and sintering process on densification and final microstructure of submicrometre alumina ceramics", *Proc. Appl. Ceram.*, **2** (2008) 13–17.
46. M.H. Fathi, M. Kharaziha, "Two-step sintering of dense, nanostructural forsterite", *Mater. Lett.*, **63** (2009) 1455–1458.
47. A. Scoton, A. Chinelatto, E.M.J.A. Pallone, A.M. Souza, M.K. Manosso, A.L. Chinelatto, R. Tomasi, "Mechanisms of microstructure control in conventional sintering", pp. 401–422 in *Sintering of Ceramics - New Emerging Techniques*, Ed. by A. Lakshmanan, InTech, Croatia, 2012.
48. X. Wang, S. Zhang, L. Li, "Piezoelectric nanoceramics", pp. 553–569 in *Springer Handbook of Nanomaterials*, Ed. by R. Vajta, Springer-Verlang, Berlin, 2013.